Bulk Reduction and Oxygen Migration in the Ceria-Based Oxides

ARTICLE *in* CHEMISTRY OF MATERIALS · FEBRUARY 2000

Impact Factor: 8.35 · DOI: 10.1021/cm991089e

5 AUTHORS, INCLUDING:

M. Saiful Islam
University of Bath
175 PUBLICATIONS **7,460** CITATIONS
SEE PROFILE

Paolo Fornasiero
Università degli Studi di Trieste
239 PUBLICATIONS **9,048** CITATIONS
SEE PROFILE

Bulk Reduction and Oxygen Migration in the Ceria-Based Oxides

Gabriele Balducci,*,† M. Saiful Islam,‡ Jan Kašpar,† Paolo Fornasiero,† and Mauro Graziani†

Dipartimento di Scienze Chimiche, Università degli Studi di Trieste, via L. Giorgieri 1, 34127 Trieste, Italy, and Department of Chemistry, University of Surrey, Guildford, Surrey GU2 5XH, U.K.

Received June 29, 1999. Revised Manuscript Received September 17, 1999

Cubic solid solutions of general formula $Ce_{1-x}M_xO_2$ (M = Zr, Th, Hf) have been modeled in the range ($0 < x < 1$) using atomistic simulation methods. The Ce^{4+}/Ce^{3+} reduction energy in the bulk materials and the activation energy for oxygen migration have been calculated. The Ce^{4+}/Ce^{3+} reduction energy decreases with increasing M content for M = Zr, Th, the most remarkable effect being displayed for M = Th. An opposite trend is obtained when M = Hf. The activation energy for oxygen migration decreases with increasing M content. The effect of Th is similar to that of Zr and consists of a substantial decrease of the activation energy at high concentrations. On the other hand, the activation energy decreases only slightly when M = Hf.

Introduction

Ceria (cerium dioxide, CeO_2) is a very attractive material in the framework of the three-way catalysts (TWCs) technology, upon which most of the automobile catalytic converters are based. One of the recognized key functions of this material is the ability of the cerium ion to switch between the Ce^{4+} and Ce^{3+} oxidation states, depending on the oxygen partial pressure of the environment:

$$CeO_2 \rightleftharpoons CeO_{2-x} + {}^1/_2 xO_2 \qquad (1)$$

Equilibrium 1 determines the so-called oxygen storage capacity of ceria, which is involved in the stabilization of the air-to-fuel ratio at the optimum stoichiometric value by releasing or consuming oxygen under "rich" or "lean" mixture conditions, respectively.[1]

Although it is now well established that addition of zirconia (zirconium dioxide, ZrO_2) to ceria to form a solid solution greatly enhances the reducibility of the Ce^{4+} ion in the bulk material,[2,3] the precise mechanism through which this occurs is still to be completely understood. Thermodynamic aspects, such as the energetics of the Ce^{4+}/Ce^{3+} reduction step and the formation of corresponding oxygen vacancies, as well as kinetic features pertaining to the transport of oxide ions from the bulk to the surface are likely to be involved. Moreover, the effects of crystal structure, phase homogeneity, textural properties, and surface area and topology have to be taken into account.

The computer simulation of oxides is a well-established tool of investigation for gaining insight into many of the chemical and physical properties of these materials.[4] We have previously used this technique to study the Ce^{4+}/Ce^{3+} reduction in the bulk and at the surface of $Ce_{1-x}Zr_xO_2$ solid solutions.[5,6] In the present paper, we extend these simulations to solid solutions of ceria with hafnia (hafnium dioxide, HfO_2) and thoria (thorium dioxide, ThO_2). Moreover, we revise some of our previously published data on the $Ce_{1-x}Zr_xO_2$ system. Our study relates largely to the energetics of Ce^{4+}/Ce^{3+} reduction and of oxygen vacancy migration as a function of the composition of the mixed oxides.

Computational Methods

The atomistic model for the simulation of ionic solids is well-established.[4] Ions are treated as classical particles bearing an electrical charge corresponding to their oxidation number. Long-range interionic Coulomb forces are handled by the Ewald technique,[7] while short-range interactions are represented by a suitably parametrized pair potential model, which in the present study had the form of a Buckingham function:

$$E_{ij} = A_{ij} \exp\left(-\frac{r_{ij}}{\rho_{ij}}\right) - \frac{C_{ij}}{r_{ij}6} \qquad (2)$$

In eq 2, E_{ij} is the short-range interaction energy between ions i and j, at distance r_{ij}. A_{ij}, ρ_{ij}, and C_{ij}

* To whom correspondence should be addressed. E-mail: balducci@univ.trieste.it.
† Università degli Studi di Trieste.
‡ University of Surrey.

(1) Taylor, K. C. Automobile catalytic converters. In *Catalysis—Science and Technology*, Anderson, J. R., Boudart, M., Eds.; Springer-Verlag: Berlin, 1984; Vol. 5.
(2) Balducci, G.; Fornasiero, P.; Di Monte, R.; Kaspar, J.; Meriani, S.; Graziani, M. *Catal. Lett.* **1995**, *33*, 193.
(3) Kundakovic, L.; Flytzani -Stephanopoulos, M. *J. Catal.* **1998**, *179*, 203−221.
(4) Catlow, C. R. A., Mackrodt, W. C., Eds. *Computer simulation of solids*; Springer: Berlin, 1982.
(5) Balducci, G.; Kaspar, J.; Fornasiero, P.; Graziani, M.; Islam, M. S.; Gale, J. D. *J. Phys. Chem. B* **1997**, *101*, 1750.
(6) Balducci, G.; Kaspar, J.; Fornasiero, P.; Graziani, M.; Islam, M. S. *J. Phys. Chem. B* **1998**, *102*, 557.
(7) Kittel, C. *Introduction to Solid State Physics*, 7th ed.; Wiley: New York, 1996.

10.1021/cm991089e CCC: $19.00
Published on Web 02/26/2000

Table 1. Potential Parameters Used to Model the Solid Solutions

Short-Range Potential Parameters: $E_{ij} = A_{ij} \exp(-r_{ij}/\rho_{ij}) - C_{ij}/r_{ij}^6$

$i-j$	A_{ij} (eV)	ρ_{ij} (Å)	C_{ij} (eV Å^6)	ref
$O^{2-}-O^{2-}$	22764.30	0.1490	27.89	25
$Ce^{4+}-O^{2-}$	1986.83	0.3511	20.40	12
$Ce^{3+}-O^{2-}$	1731.62	0.3637	14.43	12
$Zr^{4+}-O^{2-}$	985.87	0.3760	0.0	25
$Hf^{4+}-O^{2-}$	1454.60	0.3500	0.0	26
$Th^{4+}-O^{2-}$	1139.70	0.3944	0.0	26

Shell Model Parameters: $E_{core-shell}(r) = (1/2)k_2r^2$

ion	shell charge (e)	k_2 (eV Å^{-2})	ref
O^{2-}	−2.077	27.290	25
Ce^{4+}	7.7	291.75	12
Ce^{3+}	7.7	291.75	12
Zr^{4+}	1.350	169.617	25
Hf^{4+}	0.0	∞	26
Th^{4+}	7.28	193.1	26

parametrize the analytic expression for the particular ionic pair and are listed in Table 1. A cutoff distance of 10.0 Å for the short-range interactions was used throughout this study. Cation−cation interactions were assumed to be purely Coulombic.

Ionic polarizability is taken into account by means of the shell model.[8] A polarizable ion is represented by a massless shell connected to an inner massive core by a harmonic spring. The integral ionic charge is properly partitioned between the shell and the core so that a dipole moment is developed when the shell moves relative to the core as a result of the force field generated by the other ions. Coupling between polarization and short-range forces is achieved by allowing the short-range interaction to act between shells only. The potential energy of the core−shell system as a function of the relative displacement r is given by

$$E_{core-shell}(r) = \frac{1}{2}k_2r^2 \qquad (3)$$

with k_2 being the harmonic constant. The shell model parameters used in this work are reported in Table 1.

Defect calculations are based on a "two-region" approach.[9] The crystal around the defect is partitioned into an inner spherical region centered on the defect and an outer region extending to infinity. In the inner region the effect of the perturbation produced by the defect on each individual ion is explicitly taken into account, while in the outer region, where the distance from the source of the perturbation is larger, ions are treated collectively, using approximations derived from continuum theory.[10] In the present work, the radius of the inner region was 11.0 Å, corresponding to about 500 ions and to a precision of ≈0.05% in the evaluated defect energies. These computational methods are efficiently coded in the GULP program,[11] which was used for all of our calculations.

The code handles the different compositions of the solid solutions by means of fractional occupancies of the cationic sites in the cubic fluorite structure; the short-range potentials are scaled accordingly. In other words, each cationic site of the solid solution is modeled as a "hybrid" M^{4+} cation, interacting with the oxide anion through a short-range potential given by the average of the potential functions of the two cations in the system. For instance, the cation−anion short-range interaction potential for the $Ce_{1-x}Th_xO_2$ system is given by

$$E_{M^{4+}-O^{2-}} = (1 - x)E_{Ce^{4+}-O^{2-}} + xE_{Th^{4+}-O^{2-}} \qquad (4)$$

The Ce^{4+}/Ce^{3+} reduction energy was evaluated according to the procedure outlined by Sayle et al.,[12] suitably adapted to take into account the mean-field approach used to model the solid solutions. It is illustrated in Table 2, where Kröger−Vink notation has been used for the point defects. The overall reduction process (step g) is decomposed into steps a−f. The energy change associated with each component step either is known from the literature or can be calculated, thus allowing the energy change for the overall reduction process to be obtained. The Ce^{4+}/Ce^{3+} reduction process (g) generates one positively charged oxygen vacancy and two negatively charged Ce^{3+} impurities. One can therefore expect them to interact, especially at high reduction degrees. We have considered two such possible interactions, represented by equations h and i and consisting of the formation of positive ($V_O^{\cdot\cdot}Ce_M'$) and neutral ($V_O^{\cdot\cdot}Ce_M'Ce_M'$)$^\times$ clusters, respectively. In our previous paper on the $Ce_{1-x}Zr_xO_2$ system,[5] the Ce^{4+}/Ce^{3+} reduction energy was incorrectly evaluated, because of an improper handling of the hybrid cationic sites. Those values are thus revised in the present paper and presented together with the new results on the $Ce_{1-x}Th_xO_2$ and $Ce_{1-x}Hf_xO_2$ systems.

The activation energy for oxygen vacancy migration was evaluated as described in our previous paper:[5] basically, the energy corresponding to the saddle point of the migration path of an oxygen ion between two nearest-neighbor vacant sites is calculated by the code with the method of rational function optimization; the formation energy for an isolated oxygen vacancy is then subtracted from this value to give an estimate of the barrier to the oxygen vacancy migration in the bulk crystal.

Results and Discussion

Structural Modeling. The reliability of the potential parameters used in the present study can be assessed by comparing those calculated with experimentally determined static properties for the systems under investigation. From our previous studies,[5] the model satisfactorily reproduces experimental lattice constants for the $Ce_{1-x}Zr_xO_2$ system. A fairly good accord is also found with the experimental values[13,14] of the lattice constants for $Ce_{1-x}Hf_xO_2$ (x = 0.1, 0.2, 0.5, 0.8), as shown in Table 3. Finally, good agreement over the

(8) Dick, B. G.; Overhauser, A. W. *Phys. Rev.* **1958**, *112*, 90.
(9) Catlow, C. R. A. Computational Techniques and Simulation of Crystal Structures. In *Solid State Chemistry: Techniques*; Clarendon Press: Oxford, U.K., 1987; Chapter 7.
(10) Mott, N. F.; Littleton, M. J. *Trans. Faraday Soc.* **1938**, *34*, 485.
(11) Gale, J. D. *J. Chem. Soc., Faraday Trans.* **1997**, *93*, 629−637.
(12) Sayle, T. X. T.; Parker, S. C.; Catlow, C. R. A. *Surf. Sci.* **1994**, *316*, 329.
(13) Zamar, F.; Trovarelli, A.; de Leitenburg, C.; Dolcetti, G. *Stud. Surf. Sci. Catal.* **1996**, *101*, 1283−1292.
(14) Malou, P.; Debray, E.; Chappey, B. C. R. *Acad. Sci., Ser. II* **1983**, *296*, 245−247.

Table 2. Component Steps of the Ce^{4+}/Ce^{3+} Reduction Process with the Corresponding Energies

	process	associated energy change
a	$2Ce_M^{\times} \rightarrow 2Ce_{\infty}^{4+} + 2V_M''''$	$2(E_{V_M''''} - E_{Ce_M^{\times}})$
b	$2Ce_{\infty}^{4+} + 2e \rightarrow 2Ce_{\infty}^{3+}$	−73.52 eV
c	$2Ce_{\infty}^{3+} + 2V_M'''' \rightarrow 2Ce_M'$	$2(E_{Ce_M'} - E_{V_M''''})$
d	$O_O^{\times} \rightarrow O_{\infty}^{2-} + V_O^{\cdot\cdot}$	$E_{V_O^{\cdot\cdot}}$
e	$O_{\infty}^{2-} \rightarrow O_{\infty} + 2e$	−7.29 eV
f	$O_{\infty} \rightarrow {}^1/_2O_2$	−2.58 eV
g	$2Ce_M^{\times} + O_O^{\times} \rightarrow 2Ce_M' + V_O^{\cdot\cdot} + {}^1/_2O_2$	$E_{Ce^{4+}/Ce^{3+}} = 2(E_{Ce_M'} - E_{Ce_M^{\times}}) + E_{V_O^{\cdot\cdot}} - 83.39$ eV
h	$V_O^{\cdot\cdot} + Ce_M' \rightarrow (V_OCe_M')^{\bullet}$	$E_{(1:1)} = E_{(V_OCe_M')^{\bullet}} - (E_{V_O^{\cdot\cdot}} + E_{Ce_M'})$
i	$V_O^{\cdot\cdot} + 2Ce_M' \rightarrow (V_OCe_MCe_M')^{x}$	$E_{(2:1)} = E_{(V_OCe_MCe_M')^{\times}} - (E_{V_O^{\cdot\cdot}} + 2E_{Ce_M'})$
j	$2Ce_M^{\times} + O_O^{\times} \rightarrow (V_OCe_M')^{\bullet} + Ce_M' + {}^1/_2O_2$	$E^{(1:1)}_{Ce^{4+}/Ce^{3+}} = E_{Ce^{4+}/Ce^{3+}} + E_{(1:1)}$
k	$2Ce_M^{x} + O_O^{x} \rightarrow (V_OCe_MCe_M')^{x} + {}^1/_2O_2$	$E^{(2:1)}_{Ce^{4+}/Ce^{3+}} = E_{Ce^{4+}/Ce^{3+}} + E_{(2:1)}$

[a] Formation of two Ce^{4+} vacancies; note that the initial state for this step corresponds to a point defect: namely, a pure Ce^{4+} impurity at a *fractionally occupied* cationic site. Ce_{∞}^{4+} stands for a Ce^{4+} cation at infinite distance from the lattice, taken as the zero energy state. [b] Fourth ionization potential of cerium. [c] Formation of two Ce^{3+} impurities. [d] Formation of an oxygen vacancy. [e] First and second electron affinity of oxygen. [f] Bond dissociation energy of oxygen. [g] Complete Ce^{4+}/Ce^{3+} reduction process in the bulk crystal with concurrent formation of an oxygen vacancy and oxygen release. [h] Formation of a (V_OCe_M') cluster with component defects in the nearest-neighbor position. [i] Formation of a $(V_OCe_MCe_M')^{\times}$ cluster with component defects in the nearest-neighbor position. [j] Ce^{4+}/Ce^{3+} reduction with concurrent formation of the (V_OCe_M') cluster. [k] Ce^{4+}/Ce^{3+} reduction with concurrent formation of the $(V_OCe_MCe_M')^{\times}$ cluster.

Table 3. Comparison of Calculated and Experimental Values of the Lattice Parameter for Cubic $Ce_{1-x}Hf_xO_2$ Solid Solutions at Different Compositions

hafnia %	a_{exp} (Å)	a_{calc} (Å)
80	5.13[a]	5.17
50	5.20[a]	5.28
20	5.30[a]/5.37[b]	5.37
10	5.38[b]	5.40

[a] From ref 13. [b] From ref 14.

whole composition range for the three mixed oxides is obtained between our calculated lattice constants and the values derived using the empirical formula of Kim,[15] based on regression analysis of available experimental data:

$$a = 5.413 + 0.220(r_{M^{4+}} - r_{Ce^{4+}}) \qquad (5)$$

where a (Å) is the lattice constant of the cubic solid solution $Ce_{1-x}M_xO_2$ and $r_{M^{4+}}$ and $r_{Ce^{4+}}$ are the ionic radii (in Å) of M^{4+} and Ce^{4+}, respectively. Figure 1 compares our calculated values with those obtained from eq 5, assuming $r_{Ce^{4+}} = 0.97$ Å, $r_{Th^{4+}} = 1.05$ Å, $r_{Zr^{4+}} = 0.84$ Å, and $r_{Hf^{4+}} = 0.83$ Å.[16] As one would expect, the lattice constant for $Ce_{1-x}M_xO_2$ decreases with increasing x for M = Zr and Hf while the opposite holds for M = Th.

To our knowledge, there are no experimental determinations of other static properties (such as dielectric or elastic constants) for the three mixed oxides. These would constitute an improved benchmark for assessing the validity of the model, owing to their stronger dependence on the potential and core−shell parameters.

Reduction Energy. As outlined in the previous section, the Ce^{4+}/Ce^{3+} reduction energy ($E_{Ce^{4+}/Ce^{4+}}$ in step g of Table 2) was evaluated by combination of the formation energies for selected point defects with appropriate atomic properties. We are aware of the uncertainties in our evaluation procedure due to the use of "free ion" ionization potentials (steps b and e in Table 2). Our main concern, however, is to understand how the overall reduction process varies with composition; for this task our evaluation schemes have proved to be reliable. Another point to be considered here is the precise nature of the reduced states in ceria, which is still uncertain to some extent. Our approach treats the Ce^{3+} state as a small polaron according to reaction g. This is in line with other studies on many transition-metal oxides, including the high T_C superconductors;[17] the merit of such an approach is that it includes a detailed account of lattice polarization and electrostatic energy, which are difficult to introduce with other methods. The final result of the procedure for the three solid solutions is shown in Figure 2. At the lowest dopant levels, the reduction energy for the three systems is similar, with ceria being the dominant component.

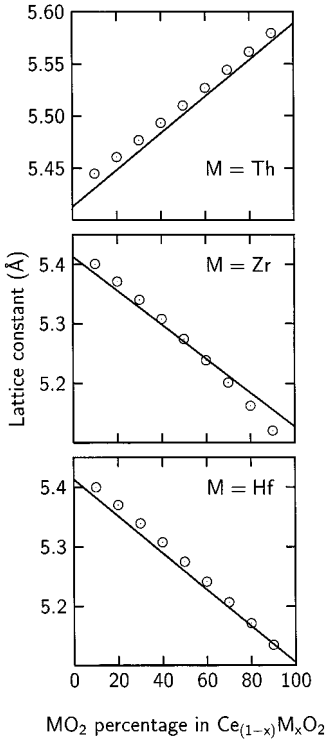

Figure 1. Comparison of calculated lattice constants (circles) with values obtained from the empirical equation (5) (lines) for the three mixed oxides.

(15) Kim, D. J. *J. Am. Ceram. Soc.* **1989**, *72*, 1415−1421.
(16) Shannon, R. D. *Acta Crystallogr.* **1976**, *A32*, 751−767.
(17) Islam, M. S.; Winch, L. J. *Phys. Rev. B* **1995**, *52*, 10510−10515.

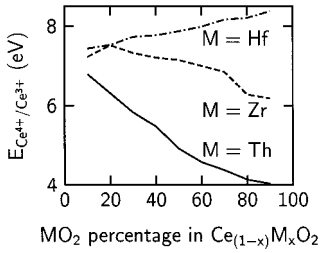

Figure 2. Ce^{4+}/Ce^{3+} reduction energy in $Ce_{1-x}M_xO_2$ for the case of no subsequent defect association ($E_{Ce^{4+}/Ce^{3+}}$ in Table 2).

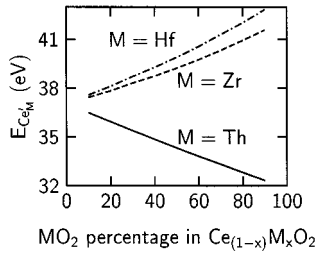

Figure 3. Formation energy for an isolated Ce'_M point defect in $Ce_{1-x}M_xO_2$.

As the dopant cation concentration increases, however, rather different trends are obtained: the Ce^{4+}/Ce^{3+} reduction energy in $Ce_{1-x}M_xO_2$ decreases for M = Th and Zr and increases for M = Hf; the decrease is more remarkable when the guest cation is Th (the trend for M = Zr which we reported in a previous paper,[5] while qualitatively similar, was biased by an incorrect treatment of the mean-field approach used to model the solid solution).

Given the classical nature of our simulations, it seems reasonable to discuss results in terms of ionic size and polarizability. Th^{4+} is considerably larger than Ce^{4+}. An increasing content of Th^{4+} in the solid solution determines an expansion of the cubic cell (Figure 1), and this can explain why the Ce^{4+}/Ce^{3+} reduction, which causes the ionic radius of cerium to increase from 0.97 to 1.14 Å,[16] is made easier. Zr^{4+} and Hf^{4+} have nearly the same size, which is smaller than that of Ce^{4+}. Hence, the increase in ionic size of cerium upon reduction is less well accommodated in this case.

This appears more clearly if one considers the formation energy for an isolated Ce'_M impurity (Figure 3): an increase with increasing dopant cation fraction is observed for Zr and Hf, while the opposite trend is obtained for Th. The same trend was obtained for every defect involving the formation of a Ce'_M center.

As can be seen in Table 1, the available potential model for Hf^{4+} does not allow for polarizability. However, from comparative calculations performed for the $Ce_{1-x}Zr_xO_2$ system by modeling the Zr^{4+} cation as an unpolarizable species, we find no significant difference between the defect energies evaluated with and without polarization terms for the Zr^{4+} cation. Indeed, cation polarizability can be expected to be much less important than oxide ion polarization in these materials.

These reduction energies are consistent with the observation that the catalytic activity is enhanced by the introduction of Zr into ceria, which is associated with increased reducibility of the bulk oxide. Temperature-programmed reduction (TPR) experiments also indicate a large bulk participation in the reduction process.[2,3] However, in contrast with our calculated Ce^{4+}/Ce^{3+} reduction energy trends, TPR measurements suggest that $Ce_{1-x}Hf_xO_2$ performs better than $Ce_{1-x}Zr_xO_2$ in terms of reducibility and oxygen storage capacity.[13] This can be interpreted as an indirect indication that other factors, such as oxygen diffusion, surface area, phase domains, grain boundary, and/or texture effects, play an important role in the overall reduction process which is observed in the TPR experiments. Indeed, if on the one hand the role of ceria and ceria-based materials in the TWC technology is now widely recognized, it is also true that the complexity of the mechanisms through which this role is effected has also emerged.[18]

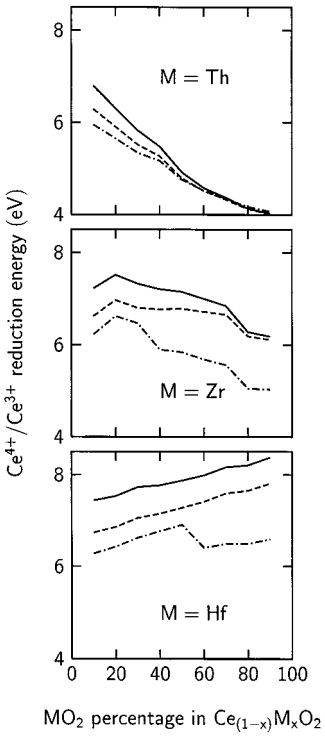

Figure 4. Effect of defect association on the Ce^{4+}/Ce^{3+} reduction energy for the three solid solutions. Different line types refer to the cases of no defect association after reduction (solid line, $E_{Ce^{4+}/Ce^{3+}}$ in Table 2, i.e., the same values of Figure 2, reported here for the sake of comparison), formation of a $(V_O^{\cdot\cdot}Ce'_M)$ cluster after reduction (dashed line, $E^{(1:1)}_{Ce^{4+}/Ce^{3+}}$ in Table 2), formation of a $(V_O^{\cdot\cdot}Ce'_MCe'_M)$ cluster after reduction (dashed−dotted line, $E^{(2:1)}_{Ce^{4+}/Ce^{3+}}$ in Table 2).

The effect of defect association on the energetics of the Ce^{4+}/Ce^{3+} reduction is shown in Figure 4, where, for each solid solution, the energy changes corresponding to steps g, j, and k of Table 2 have been plotted against guest cation fraction. As can be seen, in every case the interaction between oxygen vacancies and reduced cerium centers produces bound states which lower the energy of the overall Ce^{4+}/Ce^{3+} reduction, with the formation of $(V_O^{\cdot\cdot}Ce'_MCe'_M)^{\times}$ trios being energetically more favorable than the formation of $(V_O^{\cdot\cdot}Ce'_M)$ pairs. In the case of the ceria−thoria mixed oxide, a decrease of the binding energy is obtained with increasing thoria fraction. Our results indicate that the formation of defect clusters increases the driving force for the Ce^{4+}/Ce^{3+} reduction. However, this is not the only consequence of defect association: in fact, one can envisage

(18) Kaspar, J.; Fornasiero, P.; Graziani, M. *Catal. Today* **1999**, *50*, 285−298.

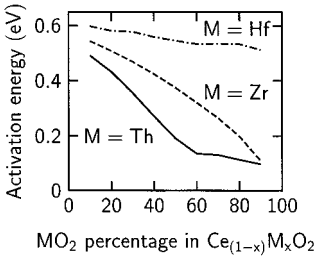

Figure 5. Activation energy for oxygen vacancy migration as a function of composition in $Ce_{1-x}M_xO_2$.

at least one additional effect, namely, the trapping of oxygen vacancies with a consequent decrease in oxygen diffusion. This is expected to become important at high degrees of reduction in these materials. The possible association between the dopant cation and a negatively charged Ce'_M defect, due to the dopant being more electronegative than Ce^{4+}, has been suggested for the ceria−thoria and ceria−zirconia systems.[19]

Oxygen Migration. When bulk ceria is reduced or oxidized via equilibrium 1, oxygen is exchanged with the environment. This means that oxygen must be able to diffuse through the lattice from the bulk toward the surface and vice versa. This appears to be the rate-determining step in isotope exchange experiments on ceria and Pt/ceria catalysts;[20] in addition, we have recently gained experimental evidence that bulk oxygen mobility limits the rate of hydrogen uptake in TPR measurements conducted on the $Ce_{0.5}Zr_{0.5}O_2$ solid solution.[21] Thus, oxygen diffusion represents a key step in the overall process, and it is of interest to study the energy changes associated with such a migration. An estimate of the activation energy for oxygen migration was obtained by evaluating the maximum of the energy profile for an oxide ion jumping between two adjacent sites of the fluorite structure, relative to the energy of an isolated oxygen vacancy. Results are reported in Figure 5 as a function of composition for the three mixed oxides (the data for $Ce_{1-x}Zr_xO_2$ are taken from our previous paper[5] and replotted here for comparison). It appears that the behavior of the ceria−thoria system is very similar to that of the ceria−zirconia solid solution, producing a substantial decrease in the energy barrier as the dopant cation concentration increases, indicating rapid oxygen transport. This high mobility of oxygen vacancies through the bulk (and to the surface) will assist in promoting the Ce^{4+}/Ce^{3+} redox cycle. For the ceria−hafnia mixed oxide, only a small decrease of the activation energy is obtained.

For each of the three systems, at all compositions, the saddle-point location for the hopping oxide ion after optimization was found to be exactly midway between the initial and final positions (i.e., at fractional coordinates ($^1/_2$, $^1/_4$, $^1/_4$) for an oxygen ion migrating from ($^1/_4$, $^1/_4$, $^1/_4$) to ($^3/_4$, $^1/_4$, $^1/_4$)). This suggests that oxygen migration takes place along the straight line connecting the two nearest-neighbor anionic positions. This is not always the case, because curved oxygen migration paths have been found in other mixed oxides.[22]

The data shown in Figure 5 suggest that thoria should have an effect comparable to that of zirconia on the bulk oxygen migration in the solid solution. Bulk oxygen diffusion has been inferred from isotope exchange measurements in $Ce_{0.1}Th_{0.9}O_2$.[23] Moreover, the value of 0.75 eV for the activation energy for oxygen migration in a $Ce_{0.993}Th_{0.007}O_2$ solid solution, derived from thermogravimetric measurements[24] is comparable with the value of 0.57 eV which can be linearly extrapolated from our calculations. We were not able to find any comparative experimental activation energies for the $Ce_{1-x}Hf_xO_2$ system.

Our results indicate that the $Ce_{1-x}Th_xO_2$ system displays features comparable with those of $Ce_{1-x}Zr_xO_2$, as far as cerium reducibility and bulk oxygen migration are concerned. However, it must be stressed that these are not the only steps involved in the overall process of oxygen buffering, and other factors may play an important role.

Conclusions

We have extended our previous calculations on the $Ce_{1-x}Zr_xO_2$ system to the $Ce_{1-x}Th_xO_2$ and $Ce_{1-x}Hf_xO_2$ solid solutions. The lattice constants of the optimized fluorite structures are in satisfactory agreement with available experimental data over the whole range of compositions. The Ce^{4+}/Ce^{3+} reduction energy in $Ce_{1-x}M_xO_2$ decreases with increasing dopant cation fraction for M = Th and Zr, while the opposite is obtained for M = Hf. The interaction between oxygen vacancies and reduced cerium centers is energetically favorable and increases the driving force for cerium reduction. The activation energy for oxygen migration in the ceria−thoria system decreases with increasing thoria content, with the trend being very similar to that already found for the ceria−zirconia solid solution. Only a small decrease is observed for the ceria−hafnia system.

Acknowledgment. MURST (Roma) "Progetti di Ricerca di Rilevante Interesse Nazionale−1998", Ministero dell'Ambiente (Contract DG 164/SCOC/97), Regione Friuli Venezia-Giulia "Fondo regionale per la ricerca", and CNR (Roma), Programmi Finalizzati "Materiali Speciali per Tecnologie Avanzate II" (Contract 97.00896.34), are gratefully acknowledged for financial support.

CM991089E

(19) Pijolat, M.; Prin, M.; Soustelle, M.; Touret, O.; Nortier, P. *J. Chem. Soc., Faraday Trans.* **1995**, *91*, 3941−3948.
(20) Holmgren, A.; Duprez, D.; Andersson, B. *J. Catal.* **1999**, *182*, 441−448.
(21) Fornasiero, P.; Kaspar, J.; Graziani, M. *Appl. Catal. B* **1999**, *22*, L11−L14.
(22) Cherry, M.; Islam, M. S.; Catlow, C. R. A. *J. Solid State Chem.* **1995**, *118*, 125−132.
(23) Grabbe, A.; Jarnagin, R. *J. Chem. Soc., Faraday Trans.* **1991**, *87*, 1259−1264.
(24) Giordano, N.; Antonucci, V.; Bart, J.; Maggiore, R. *Z. Anorg. Allg. Chem.* **1982**, *484*, 195−202.
(25) Dwivedi, A.; Cormack, A. N. *Philos. Mag. A* **1990**, *61*, 1.
(26) Lewis, G. V.; Catlow, C. R. A. *J. Phys. C* **1985**, *18*, 1149.